Research Article

Hao Yang*, Xin Wang, Yimeng Duan, Haotian Zhang, Miaomiao Chen, and Xinyu Wang

Ab initio molecular dynamics of insulating paper: Mechanism of insulating paper cellobiose cracking at transient high temperature

https://doi.org/10.1515/epoly-2023-0055
received May 22, 2023; accepted July 11, 2023

Abstract: Oil-impregnated paper is the most widely used insulating material for power transformers. Power transformers inevitably generate a lot of heat during operation. Among them, thermal aging is one of the main forms of aging for insulating paper. In this study, the *ab initio* molecular dynamics method based on the density functional theory is used to simulate the cracking mechanism of cellobiose under transient high temperature. The results show that the cellobiose is relatively stable at 343 K, the motility of the cellobiose is enhanced at 1,800 K, the cellobiose starts to decompose at 2,400 K, and new characteristic products are formed at 3,000 K. The characteristic products include CO, H_2O, CH_3OH, H_2, and CH_4. These characteristic products can represent the degree of cracking of insulating paper. Therefore, it is necessary to explore the mechanism of cracking of insulating paper caused by transient high temperature.

Keywords: pyrolysis, molecular dynamics, density functional, characteristic products

1 Introduction

Power transformer is one of the main power equipment in the power system that plays a role in transformation of electrical energy (1), and oil-paper insulation is the main insulation medium in today's high-voltage transformers (2,3). In actual operation, insulating paper inside the transformer will generate a lot of heat (4), and thermal aging is the main form of deterioration of insulating paper in various aging forms (5). A large number of studies on the thermal aging of transformer oil-paper insulation have focused on the long-term aging process of the insulating paper, such as extracting characteristic parameters to generalize the aging law based on macroscopic accelerated aging experiments. The International Electrotechnical Commission points out that the physical and chemical performance parameters of oil-paper insulation system itself can be used as the characteristic quantity of aging evaluation during the aging process of transformer (6). The main characteristic parameters include dissolved gas analysis in transformer oil (7), tensile strength and degree of polymerization (DP) of insulation paper, and furfural content in oil (8,9). The DP is often used in previous studies to describe the structural integrity of the insulating paper, with a DP of 500, indicating that the paper is in the middle of its life, and a DP as low as 250 requiring immediate replacement with new paper (10–12). The process of thermal aging of insulating paper is complex, and the mechanism of chemical reactions in the condensed phase of pyrolysis is a key to a comprehensive understanding of cellulose pyrolysis (13). In recent years, a number of scholars have attempted to explore the stability of cellulose itself, complementing experimental data on cellulose pyrolysis with electronic structure calculations and molecular simulations (14–18). This allows the capture of individual chemical reactions that occur during decomposition (19–22). To explore the properties of cellulose, numerous studies have been carried out by scholars using molecular dynamics methods based on conventional mechanics. Due to the different physical and chemical properties of the crystalline and amorphous regions of cellulose (23), each part of the cellulose has different stability (24,25). In addition to the properties of cellulose itself, which affect the stability of insulating paper, temperature is also a major factor (26,27). To further understand the stability of insulating cellulose at the microscopic level, previous authors have investigated the cracking mechanism of insulating cellulose based on quantum mechanical methods. The formation and disappearance of chemical bonds, which act as bridges connecting

*** Corresponding author: Hao Yang,** School of Electronics and Information, Xian Polytechnic University, Xi'an 710048, China; School of Electrical Engineering, Xi'an Jiaotong University, Xi'an 710049, China, e-mail: yanghao@xpu.edu.cn
Xin Wang, Yimeng Duan, Haotian Zhang, Miaomiao Chen, Xinyu Wang: School of Electronics and Information, Xian Polytechnic University, Xi'an 710048, China

atoms, directly affect the stability of cellulose itself. Moreover, the interaction of the aging product with its own atoms will directly lead to the formation and loss of chemical bonds (28,29). The integrity of the chemical bond between the glycosidic bond and the pyran ring in the cellobiose directly determines the DP of cellulose in the insulating paper (15,23).

However, the mechanism of cracking at transient high temperature has not yet been elucidated. Transient high temperature can easily cause local damage to the insulating paper. When the insulation paper has a fault similar to the point defect, the local insulation performance of the insulation paper will be greatly reduced. The point defects are the beginning of the cracking of the insulating paper. Therefore, it is necessary to carry out a theoretical study of the mechanism of thermal cracking at transient high temperature. In this article, the radial distribution function (RDF) method is used to verify the effect of instantaneous high temperature on the cellulose of insulating paper. The mechanism of thermal cracking at transient high temperature is explained by the *ab initio* molecular dynamics from the perspective of bond breaking and atom bonding. As the earliest characteristic product, CH_3OH can be used as an important indicator of the early aging of insulating paper (DP > 900) (30,31). The content of CO and H_2O can be used as the characteristic gas to detect the degree of decomposition inside the insulating paper (32). This also makes up for the theoretical gap that the furfural can only be used to monitor the aging state of the insulating paper at intermediate and late stages, but not at early stages (33).

2 Theory and simulation details

2.1 Calculation theory

The calculation of electronic ground state is a complex quantum many-body problem. Density functional theory can reduce the calculation amount on the basis of ensuring the calculation accuracy (34). The Ab initio molecular dynamics method is based on density functional theory to transform complex multibody problems into a set of self-consistent single-electron orbital equations (35,36). Compared with conventional molecular dynamics simulations, *ab initio* molecular dynamics is computationally more accurate, takes longer to compute, and is computationally more expensive. Therefore, *ab initio* molecular dynamics is more suitable for the calculation of small molecular systems. However, insulating paper cellulose is a type of polymer, and the aging process can take years under natural conditions. To reduce the simulation timescale and ensure the accuracy of the simulation, a reasonably high temperature should be set during the simulation to accurately predict the pyrolytic behavior of cellulose molecules in insulator paper under transient high temperature.

2.2 Simulation details settings

Cellobiose molecules are the basic skeleton of cellulose in insulating paper, which is polymerized from cellulose. The cellobiose model is constructed by Materials Studio, and the periodic boundary conditions are established with a box size of 18 × 18 × 18 Å. As shown in Figure 1, the configuration is first geometrically optimized to approximate the exchange-correlation potential using generalized gradient correction and Perdew–Bruke–Ernzerhof (PBE) function (37,38). In view of the importance of the long-range dispersion correction for weakly interacting systems, the Grimme dispersion correction is added to the PBE generalization function. Ab initio molecular dynamics simulation is performed when the geometric optimization converged. The 5 ps kinetic simulations are performed for the cellobiose model under an isothermal-isochoric (NVT) ensemble systems as well as a Nose–Hoover thermostat to bring the system to equilibrium at 298.15 K (39). The equilibrated system is then subjected to 15 ps Ab initio molecular dynamics simulation at 343, 1,800, 2,400, and 3,000 K, respectively.

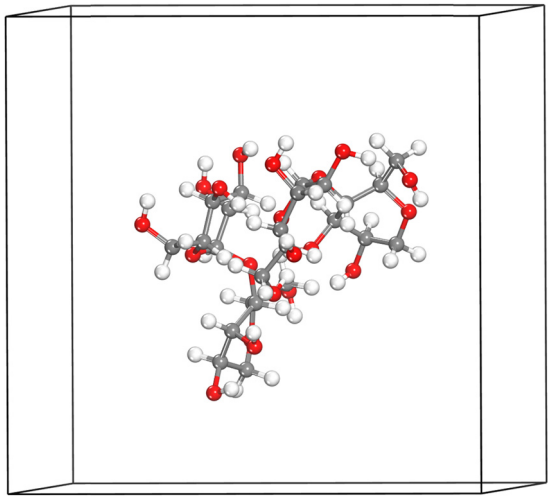

Figure 1: Cellobiose model with boundary conditions.

3 Results and discussion

3.1 Effect of transient high temperature on thermal cracking

The pyran rings are the main skeleton of the cytosol, where the C–C and C–O bonds are the main building blocks of the pyran rings, and the C–O bond is also the main chemical bond forming the glycosidic bond. At the same time, hydrogen bonding also plays a crucial role in the stability of cellulose, where hydrogen bonding is mainly caused by hydroxyl groups. In particular, it is important to investigate the stability of the C–C bond, the C–O bond, and the O–H bond.

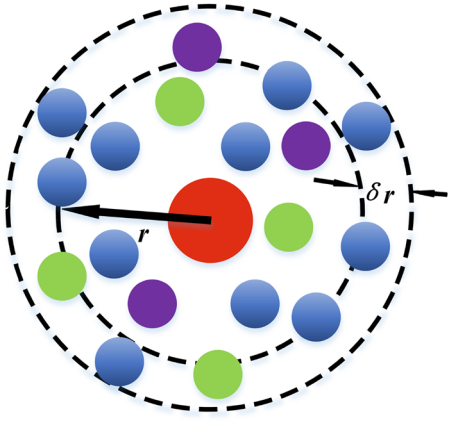

Figure 2: Summary diagram of radial distribution function.

RDFs are often used to describe the probability of occurrence of other particles around a certain particle in a dynamical problem. The stability of the chemical bonds of cellobiose molecules can be explored by plotting the RDF of different chemical bonds at the corresponding temperatures separately using VMD software. The equation used to calculate the RDF is shown in Eq. 1 (40), where $g(r)$ is a function describing the density of particles at a certain distance from the reference particle, which reflects the probability of finding another particle in a spherical space with radius from r to $r + \delta r$, and V is the volume of the system; moreover, N is the number of atoms. We can see a summary diagram of the RDF in Figure 2.

$$g(r) = \frac{2V}{N^2}\left[\sum \delta(r - r_{ij})\right] \tag{1}$$

As shown in Figure 3, the horizontal axis r in the four plots represents the interatomic distance and the vertical axis $g(r)$ represents the particle distribution probability. The valence r corresponding to the peak of each curve is exactly the number of corresponding bond lengths corresponding to Table 1. As the temperature increases, the value of the award distribution function for each chemical bond decreases, and

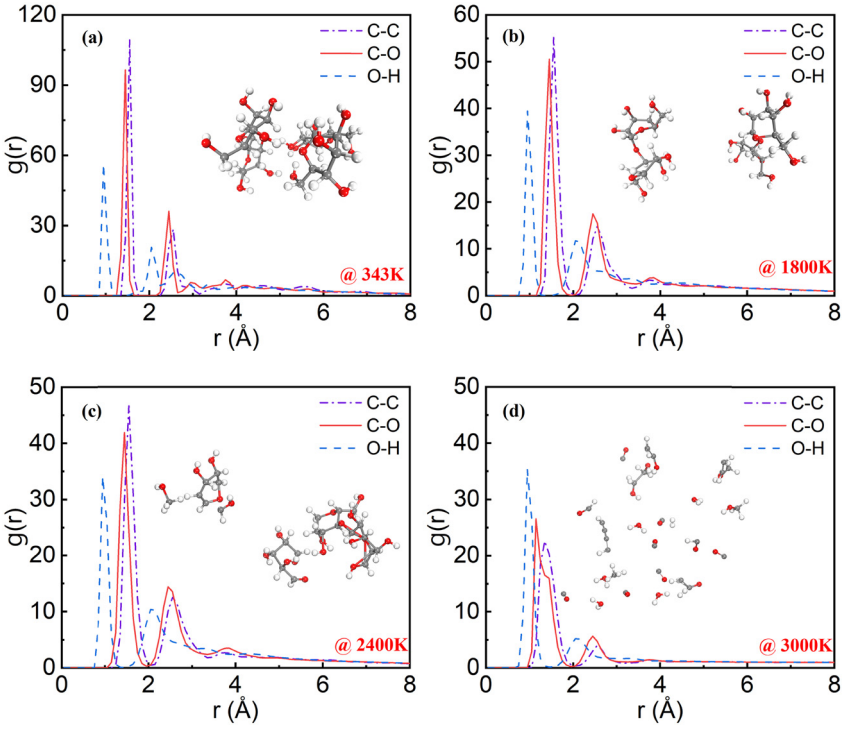

Figure 3: Radial distribution functions of C–C, C–O, and C–H bonds at (a) 343, (b) 1,800, (c) 2,400, and (d) 3,000 K.

Table 1: Bond energy and bond length of C–C, C–O, and O–H bonds

	C–C bond	C–O bond	O–H bond
Length of bond (Å)	1.54	1.43	0.96
Energy of bonds (kJ·mol^{-1})	332	326	464

temperature is able to influence the composition of these three types of chemical bonds. Among the four temperatures, the RDF values of the three bonds are the largest at 343 K. Although the RDF values of the three bonds at 1,800 K change much compared with 343 K, the bonds are not broken. It can be seen that the transient high temperature enhances the kinetic activity of the cellobiose. The increasing distance between cellobiose molecules is not conducive to polymerization. At temperatures below 2,400 K, the same temperature basically follows the largest value of the RDF for the C–C bond, followed by the C–O bond, and the smallest value of the RDF for the O–H bond, which also indicates that the temperature below 2,400 K has less effect on the basic skeleton of the cellobiose. When the temperature reaches 3,000 K, the values of the RDFs for the different chemical bonds change, with the largest changes for the C–C bond and the C–O bond, indicating that the temperature affects the C–C bond and the C–O bond much more than the O–H bond. This is also related to the bond energy and length, as shown in Table 1. The C–C and C–O bonds have similar energies and are much smaller than the O–H bond. The smaller the bond energy, the easier it is to be broken.

3.2 Analysis of cellobiose bond breaking and characteristic product generation process

3.2.1 Cellobiose bond-breaking process

From Figures 4a and 5a, it can be seen that the glycosidic bond breaking, pyran ring opening, and C–C bond breaking of the C atoms attached to the glycosidic alcohols mainly occur at 2,400 K in cellobiose. At 11.432 ps, the glycosidic bond C_{23}–O_{31} is broken first and the cellobiose split. The C_4–O_5 bond and the pyran ring are broken at 11.542 ps. Two C–C chemical bonds, C_{10}–C_6 and C_{28}–C_{32}, are broken at 11.78 ps and 11.81 ps, respectively. When the simulation time increased to 12.788 ps, C_{32}–H_{42} is broken. In summary, it is not difficult to find the order of bond breaking in this order, C–O bond, C–C bond, C–H bond, consistent with the law of variation for different bond energy sizes in Table 1. It is clear that the main structure of the cell body is fully cleaved. When the temperature reaches or even exceeds 2,400 K, the transient high temperature immediately causes the bonds of cellulose to break.

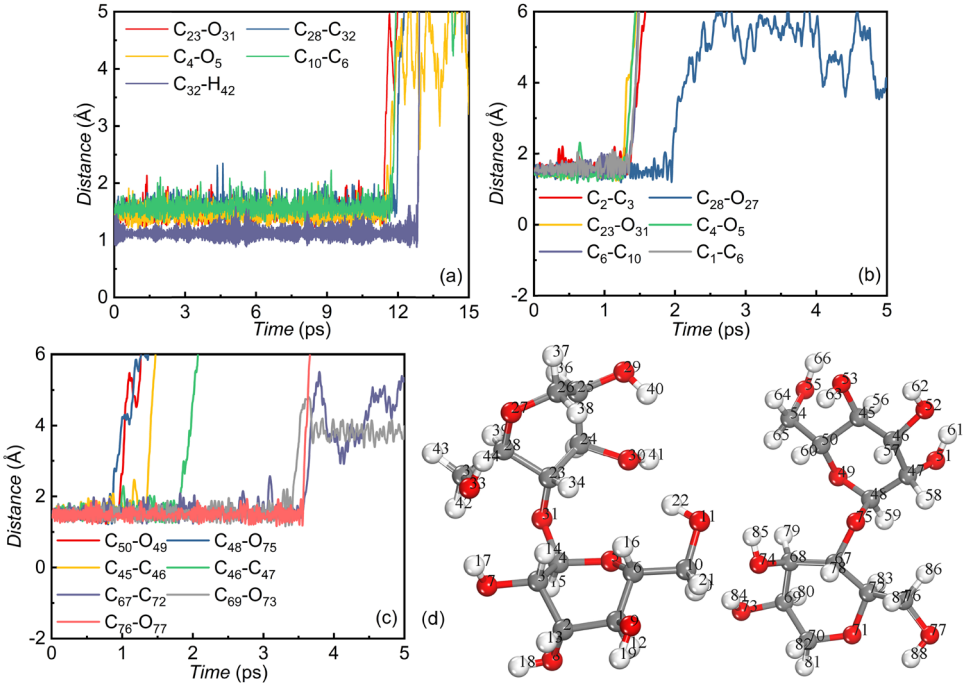

Figure 4: (a) Bond breaking of cellobiose at 2,400 K. (b) and (c) Bond breaking of two cellobiose molecules at 3,000 K. (d) Atomic serial number and corresponding atom.

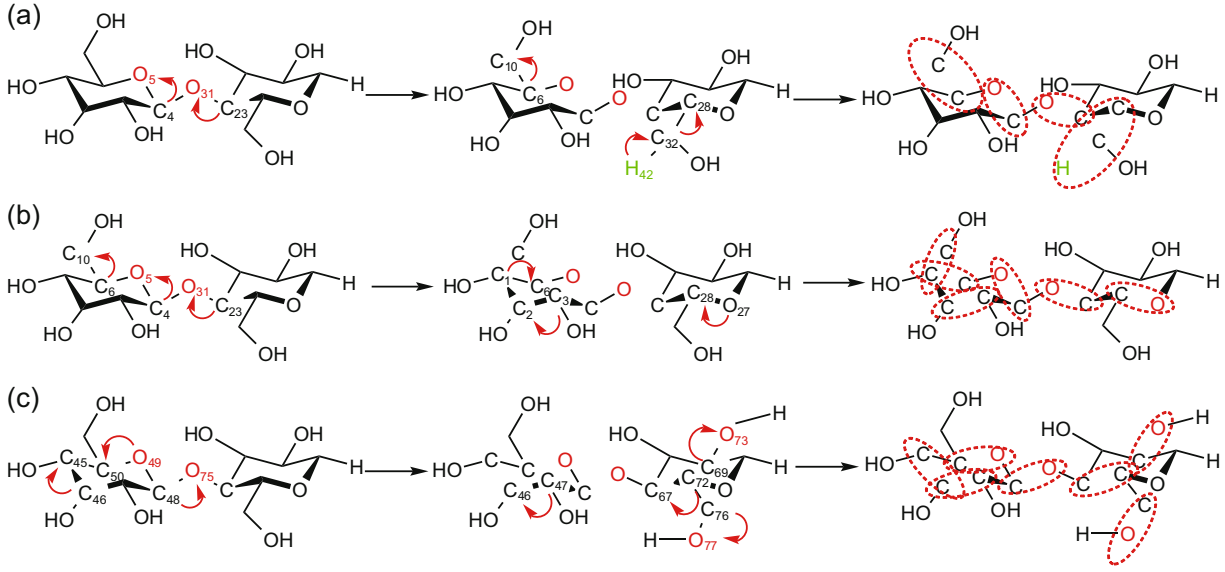

Figure 5: (a) Diagram of cellobiose cleavage process at 2,400 K. (b) and (c) Diagram of cellobiose cleavage process at 3,000 K.

As shown in Figures 4b and 5b, the glycoside bond C_{23}–O_{31} breaks at 3,000 K and 1.283 ps. The C_4–O_5 bond on the pyran ring breaks at 1.319 ps, which also marks the opening of the pyran ring. Then a lot of C–O, C–C bonds crack. Meanwhile, the cleavage process of another cellobiose at 3,000 K can be seen in Figures 4c and 5c. The glucoside bond C_{48}–O_{75} breaks first at 0.874 ps. At a time of 0.974 ps, the C_{50}–O_{49} bond on the pyran ring breaks. A large number of C–O bonds and many C–C bonds crack after 1.158 ps.

It is found that the glucoside bond, as the weakest chemical bond, breaks first by comparing the cleavage of cellobiose at 2,400 and 3,000 K. This is also one of the main factors that reduces the DP of insulating paper under extreme conditions. Second, the C–O bond on the pyrane ring also breaks immediately after the glycoside bond. The service life of insulating paper is determined by the opening of the pyran ring and the breaking of the glycoside bond.

3.2.2 Analysis of characteristic product generation process

Instantaneous high temperature not only causes thermal cracking of cellobiose but also produces new characteristic products. To explore the mechanism of cracking, the generation process of various products is described in detail at 3,000 K.

3.2.2.1 The formation of H_2O molecules

The two sources of H_2O molecules are shown in Figure 7a and b. Figure 6a shows that the C_{70}–H_{82} chemical bond breaks at 3.434 ps and the H_{82} atom is shed. This is immediately followed by the C_{76}–O_{77} bond breaking at 3.533 ps, and the primary alcohol hydroxyl O_{77}–H_{88} is shed. The detached primary alcohol

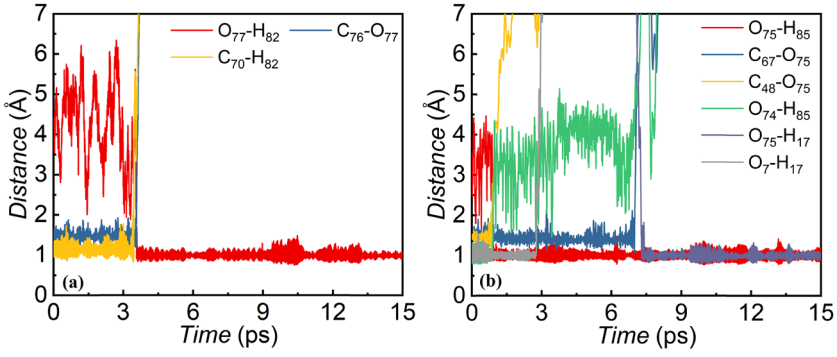

Figure 6: AIMD simulation of the variation of bond length with time for cellobiose broken bonds of insulating paper and H_2O bonding.

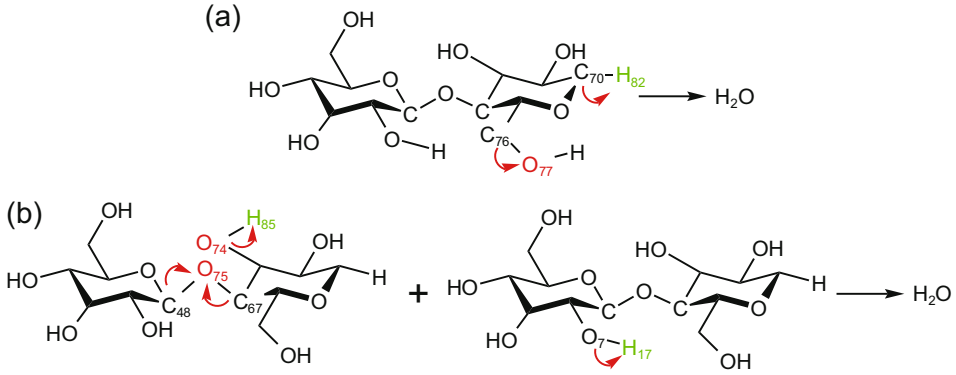

Figure 7: (a) The primary alcohol hydroxyl group combines with the H atom on the pyran ring to form H_2O. (b) The glycoside bond breaks and dehydrogenates the secondary alcohol hydroxyl group to form H_2O.

hydroxyl group O_{77}–H_{82} forms a H_2O molecule with the H_{82} atom at 3.592 ps. Figure 7a demonstrates the origin of the radicals in the H_2O molecule, where the primary alcohol hydroxyl group combines with the H atom on the pyran ring to form H_2O.

The H_2O molecule shown in Figure 7b is formed by the interaction of two cellobiose molecules. Figure 6b shows that C_{48}–O_{75} breaks at 0.873 ps causing O_{75} to fall off, while the strong electronegativity of the oxygen atom attracts the H_{85} atom that has not yet broken. The O_{75}–H_{85} bond breaking occurs at 0.894 ps. The broken H_{85} atom immediately combines with the O_{75} atom to form an O–H bond. The time increases to 2.773 ps when the O_7–H_{17} bond breaks, dislodging the H_{17} atom. The C_{67}–O_{75} bond is broken when the simulation time reaches 7.014 ps, allowing the O_{75}–H_{85} to completely detach from the cellobiose. At 7.275 ps, O_{75}–H_{17} binds to form a chemical bond, at which point the H_2O molecule is fully formed. The H_2O molecule formation process is dominated by C–O bonding, O–H bond breaking, and the formation of new O–H bonds. There is a direct link between the formation of H_2O molecules and the breaking of one of the glycosidic bonds of the cytosol, which is completely broken.

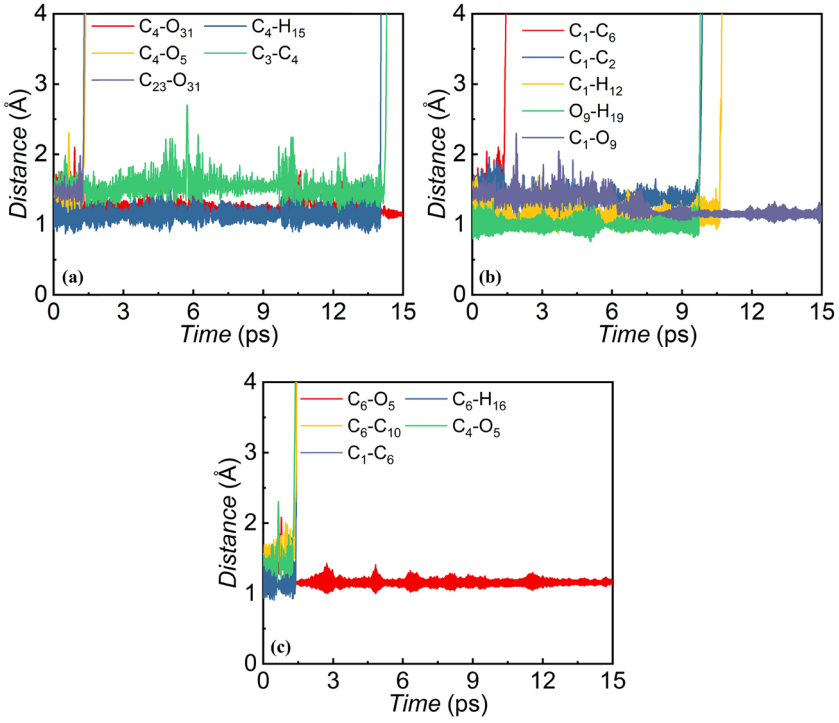

Figure 8: AIMD simulation of the variation of bond length with time for cellobiose broken bonds and CO bonding of insulating paper.

This also reflects the fact that the amount of dissolved H_2O in oil in oil-immersed transformers is one of the measures to characterize the degree of aging of insulating paper. In the formation of both H_2O molecules, it was found that when the C–O bond is broken, the O atoms in the secondary alcohol hydroxyl group are more electronegative and also more likely to cause hydrogen capture and dehydration of the O atoms.

3.2.2.2 The formation of CO

The formation process of CO is complex, and the three different pathways of CO cleavage are illustrated in Figure 9a–c. The bond breakage of C_{23}–O_{31} at 1.274 ps shown in Figure 8a marks the glycosidic bond damage. Immediately, the bond breaking at 1.311 ps occurs at C_4–O_5, and since C_4–O_5 is a component of the pyran ring, the pyran ring opens at this point. The formation of CO is closely related to the glycosidic bond and the pyran ring as shown in Figure 9a, which requires both glycosidic bond breakage and pyran ring opening to form CO, and the C–O bond is derived from the glycosidic bond.

The formation of CO is shown in Figure 8b, where the C_1–C_6 bond breaks at 1.378 ps causing the pyran ring to open. The C_1–C_2 bond is broken at 9.769 and 9.731 ps, respectively. The C_1–H_{12} bond breaks when the simulation time reaches 10.626 ps, allowing C_1–O_9 to be free to form CO. It can also be seen from Figure 9b that the two C–C

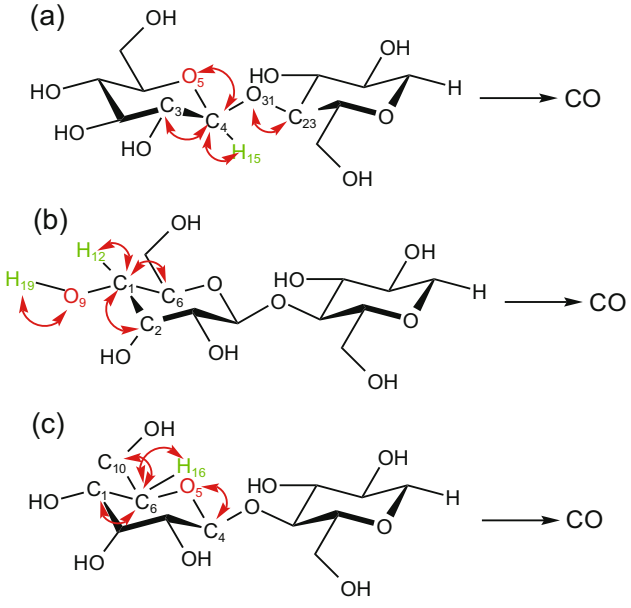

Figure 9: (a) The C–O bond on the glycoside bond dissociates to form CO. (b) The C atom on the pyran ring dissociates with the O atom on the hydroxyl group to form CO. (c) The C–O bond on the pyran ring dissociates to form CO.

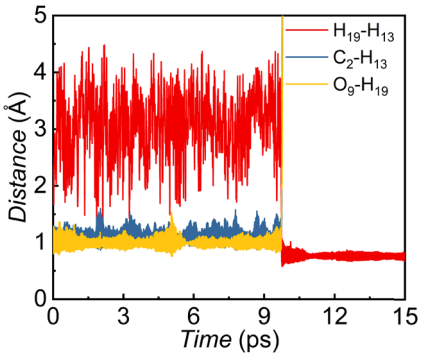

Figure 10: AIMD simulation of the variation of bond length with time for cellobiose broken bonds and H_2 bond formation in insulating paper.

bonds on the pyran ring break first causing the pyran ring to open, followed by the H atom on the C atom of the secondary alcohol shedding the H atom on the attached hydroxyl group to eventually form CO. The formation of this type of CO is related to the O atom on the pyran ring and the hydroxyl group.

The chemical bonds C_4–O_5, C_1–C_6, C_6–C_{10}, and C_6–H_{16} are broken within 1.317–1.416 ps in Figure 8c, respectively, and C_6–O_5 on the pyran ring broke off to form CO. As shown in Figure 9c, the C–O bonds on the pyran ring are broken successively with the chemical bonds formed by the surrounding atoms. Finally, the C–O bond on the pyran ring breaks free to form CO. In summary, there are three ways of CO formation, which are formed by the C–O bond on the glycosidic bond, the C atom of the secondary alcohol on the pyran ring with the O atom on the attached hydroxyl group, and the C–O bond on the pyran ring breaking free.

3.2.2.3 The formation process of H_2

Figure 10 depicts the formation of H_2. The C_2–H_{13}, O_9–H_{19} chemical bond is broken at 9.737 ps when the cellobiose is continuously cleaved at a transient high temperature. The two free H atoms combine to form H_2. Figure 11 shows a schematic diagram of the source of hydrogen H_2, where the seco-alcohol C atom on the pyran ring is dehydrogenated; the adjacent seco-alcohol C atom is dehydrogenated

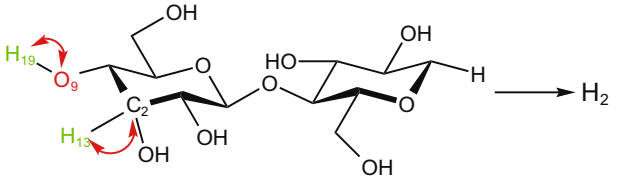

Figure 11: The H atom on the hydroxyl group combines with the H atom attached to the C atom in the pyran ring to form H_2.

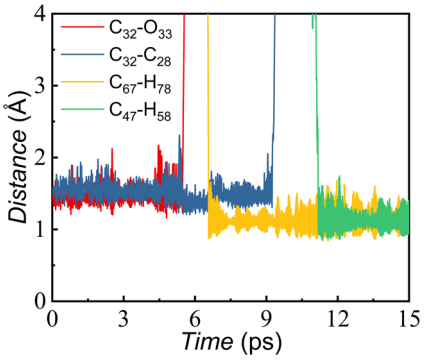

Figure 12: AIMD simulation of the variation of bond length with time for cellobiose broken bonds and CH_4 bond formation in insulating paper.

by attachment to the hydroxyl group; and the two free H atoms combine to form H_2.

3.2.2.4 The formation process of CH_4

The methane formation process is represented in Figure 12. The C_{32}–O_{33} bond is broken when the cleavage time reaches 5.5 ps. The hydrogen atom H_{78} then forms a new bond with the carbon atom C_{32} at 6.566 ps. The C_{32}–C_{28} bond is broken at 9.315 ps, when the C_{32} valence electron is in an unsaturated state. The free methyl group forms a new C–H bond with the hydrogen atoms H_{58} and H_{78} at 11.173 and 6.601 ps, respectively. The methane molecule is formed. The CH_4 radical shown in Figure 13 is associated with the source of the constituent atoms. The C–O bond formed by the C atom of the primary alcohol with the attached hydroxyl group and the C–C bond formed with the C atom on the pyran ring break at high temperatures. Afterward, the C atom of the glycosidic bond of the other cellobiose sheds an H atom, the C atom on the pyran ring sheds an H atom, and the free two H atoms combine with the C atom of the secondary alcohol to form methane CH_4.

3.2.2.5 The formation of CH_3OH

The formation process of CH_3OH can be divided into two categories, one is the shedding and reorganization of the cellobiose own atoms and radicals. From Figure 14a, it can be seen that the simulation time breaks the C_{10}–C_6 and C_6–H_{16} chemical bonds at 1.357 ps and 1.403 ps, respectively, and the free H_{16} forms a new chemical bond with C_{10}. Figure 15a shows that the C–C bond formed by the C atom of the primary alcohol with the C atom on the pyran ring breaks, and the C–H bond formed by the H atom attached to the C atom on the pyran ring breaks, and the shed methanol group CH_2OH combines with the H atom to produce CH_3OH.

The other category is the free combination of two cellobiose molecules with their own atoms shedding free radicals. Figure 14b shows the formation process of the second type of methanol molecule. The first to break the bond is C_{50}–C_{54}, and the valence electron layer, which is originally

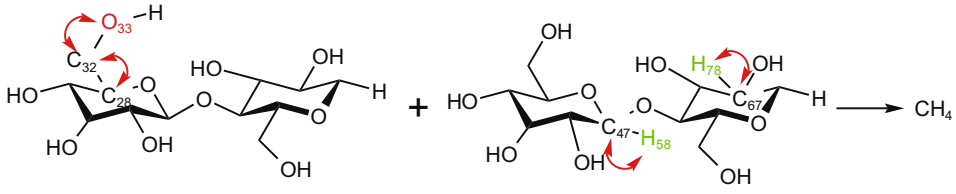

Figure 13: The free radical CH_2 from the primary alcohol C atom combines with the H atom from the secondary alcohol C atom to form CH_4.

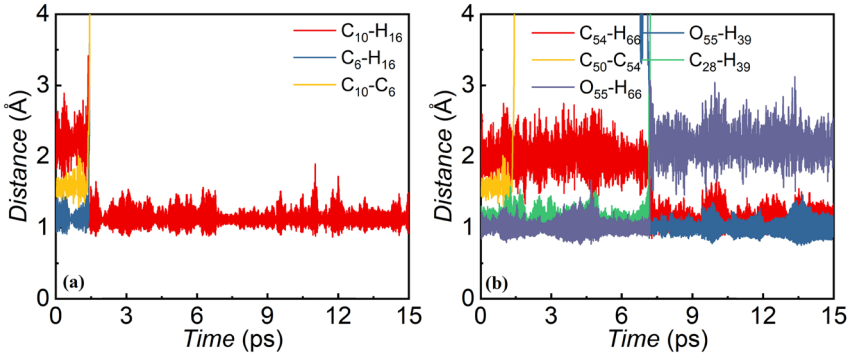

Figure 14: AIMD simulation of the variation of bond length with time for cellobiose broken bonds and CH_3OH bond formation in insulating paper.

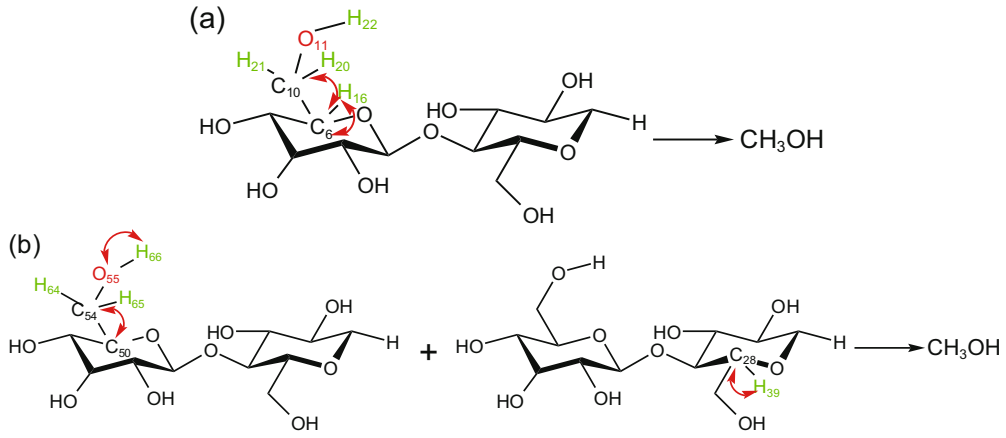

Figure 15: (a) After the C–C bond of primary alcohol is broken and dissociated, a free radical is generated and bonded with its own hydrogen atom to form CH_3OH. (b) The primary alcohol C–C bond breaks and dissociates, resulting in a free radical that combines with the hydrogen atom of another cellobiose to form CH_3OH.

saturated with C_{54}, is no longer stable. With time, several chemical bonds are broken, and new bonds are formed between 7.1 and 7.2 ps. H_{66} on O_{55} is freed and bonds with C_{54}, and the valence electron layer of C_{54} reaches stable saturation again. O_{55} captures the H_{39} atom on C_{28}, and a new O–H bond is formed after the C–H bond is broken. Figure 15b shows the origin of the composition of this type of methanol molecule. The C–C bond consisting of the C atom of the primary alcohol and the C atom on the pyran ring breaks, along with a break in the primary alcohol hydroxyl group. The C atom on the pyran ring of another cellobiose breaks the C–H bond with the attached H atom, and a bond break occurs in the own primary alcohol hydroxyl group. The free radical CH_2O combines with the detached H atom to form a new chemical bond, allowing the formation of the methanol molecule CH_3OH.

The main products of cellulose at instantaneous high temperatures are shown in Figure 16. The highest content of H_2O and CO is followed by hydrogen H_2 and CH_3OH, and the lowest content is methane CH_4. Insulating paper is the only source of CH_3OH in oiled paper insulation system.

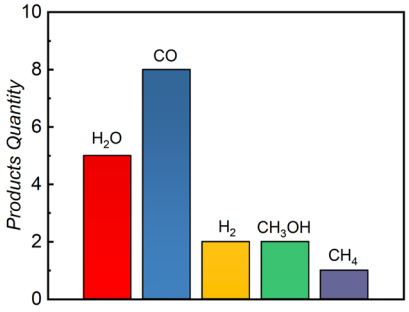

Figure 16: Diagram of product content.

Even though there is less CH_3OH after thermal cracking of insulating paper, CH_3OH is the first to be produced by insulating paper under instantaneous high temperature. Therefore, the content of CO, H_2O, and CH_3OH, and the rate of CH_3OH production can be used to monitor partial discharge faults.

4 Conclusions

In this study, the influence of transient high temperature on thermal cracking of insulating paper is explored. In this simulation, it is found that when the temperature is higher than 2,400 K, the glycosidic bond and pyran ring would first crack in a short time. The primary source of H_2O is the glycosidic bond. The strong electronegativity of the O atom is also the main driving force for the formation of H_2O. Dehydration will cause a rapid decline in the DP of insulating paper. CO is mainly derived from the C–O bond on the glycosidic bond and the C–O bond on the pyran ring. The production of a large amount of CO proves that the pyranoid ring is heavily cleaved. Therefore, the content of H_2O and CO can directly explain the degree of thermal cracking of insulating paper. H_2 and CH_4 are produced in a similar process, both of which are formed by the recombination of atoms and chemical bonds connected to the pyran ring. CH_3OH is formed by breaking the bond between C atom of primary alcohol on the pyran ring and C atom on the pyran ring and combining with H atom. The presence of CH_3OH confirms that the chemical bond to the pyran ring is not stable. In addition to cracking of the glycosidic bond and the main body of the pyran ring, the

part connected to the main body will also be largely cracked. Finally, the insulating paper loses its insulation property at instantaneous high temperature. As a result, transient high temperature will cause thermal cracking of insulating paper. Glycosidic bond, pyran ring, and the broken bond recombination of atoms and chemical bonds connected with the pyran ring result in thermal cracking of insulating paper. This study also shows that the content of CO, H_2O, and CH_3OH as well as the CH_3OH production rate is a feasible method to detect partial point defects. CH_3OH is a unique cracking product of insulating paper. By monitoring CH_3OH, the operating conditions of the insulating paper can be determined earlier. This will be conducive to the improvement of power quality and the long-term stable operation of the power system.

Funding information: This work was supported by The National Natural Science Foundation of China (52007138) and Key Research and Development Program of Shaanxi Province (2023-YBGY-070).

Author contributions: Hao Yang: writing – review and editing; Xin Wang: writing – original draft and formal analysis; Yimeng Duan: data curation and methodology; Haotian Zhang: data curation and methodology; Miaomiao Chen: conceptualization; Xinyu Wang: investigation. All the authors have read the paper and commented on the text.

Conflict of interest: The authors state no conflict of interest.

Data availability statement: All data in this article can be obtained by contacting the corresponding author.

References

(1) Bakar NA, Abu-Siada A, Islam S. A review on chemical diagnosis techniques for transformer paper insulation degradation. IEEE Power Engineering Conference; 2014. doi: 10.1109/AUPEC.2013.6725476.

(2) Cui HZ, Yang LQ, Zhu YW, Li ST, Abu-Siada A, Islam S. A comprehensive analyses of aging characteristics of oil-paper insulation system in HVDC converter transformers. IEEE Trans Dielectr Electr Insulation. 2020;27(5):1707–14. doi: 10.1109/TDEI.2020.008788.

(3) Murugan R, Ramasamy R. Understanding the power transformer component failures for health index-based maintenance planning in electric utilities. Eng Fail Anal. 2018;96:274–88. doi: 10.1016/j.engfailanal.2018.10.011.

(4) Hussain MR, Refaat SS, Abu-Rub H. Overview and partial discharge analysis of power transformers: A literature review. IEEE Access. 2021;9:64587–605. doi: 10.1109/ACCESS.2021.3075288.

(5) Liao RJ, Lin YD, Guo P, Liu HB, Xia HH. Thermal aging effects on the moisture equilibrium curves of mineral and mixed oil-paper insulation systems. IEEE Trans Dielectr & Electr Insulation. 2015;22(2):842–50. doi: 10.1109/TDEI.2015.7076783.

(6) International Electrotechnical Commission. Ageing Procedures and Evaluation of Test Results. Geneva: IX-IEC; 2001.

(7) Xia GQ, Wu GN, Gao B, Yin HJ, Yang FB. A new method for evaluating moisture content and aging degree of transformer oil-paper insulation based on frequency domain spectroscopy. Energies. 2017;10(8):1195. doi: 10.3390/en10081195.

(8) Ghoneim S, Taha I. A new approach of DGA interpretation technique for transformer fault diagnosis. Int J Electr Power & Energy Syst. 2016;81:265–74. doi: 10.1016/j.ijepes.2016.02.018.

(9) Duval M, Pablo DA, Atanasova-Hoehlein I, Grisaru M. Significance and detection of very low degree of polymerization of paper in transformers. IEEE Electr Insulation Mag. 2017;33(1):31–8. doi: 10.1109/MEI.2017.7804314.

(10) Oommen TV. Cellulose insulation materials evaluated by degree of polymerization measurements. In: Proc.elect./electron.insul.conf; 1981. p. 257–61.

(11) Ali M, Eley C. Measuring and understanding the ageing of kraft insulating paper in power transformers. IEEE Electr Insulation Mag. 1996;12(3):28–34. doi: 10.1109/57.509922.

(12) Shang Y, Yang L, Guo ZJ, Yan Z. Assessing aging of large transformers by furfural investigation. In: ICSD'01. Proceedings of the 20001 IEEE 7th International Conference on Solid Dielectrics; 2001. p. 272–4.

(13) Mettler MS, Vlachos DG, Dauenhauer PJ. Top ten fundamental challenges of biomass pyrolysis for biofuels. Energy & Environ Sci. 2012;5(7):7797–809. doi: 10.1039/c2ee21679e.

(14) Liu C, Huang J, Huang X, Li H, Zhang Z. Theoretical studies on formation mechanisms of CO and CO_2 in cellulose pyrolysis. Computational Theor Chem. 2011;964(1–3):207–12. doi: 10.1016/j.comptc.2010.12.027.

(15) Zhang X, Li J, Yang W, Blasiak W. Formation Mechanism of Levoglucosan and Formaldehyde during cellulose pyrolysis. Energy & Fuels. 2011;25(Jul–Aug):3739–46. doi: 10.1021/ef2005139.

(16) Mayes HB, Broadbelt LJ. Unraveling the reactions that unravel cellulose. J Phys Chem A. 2012;116(26):7098–106. doi: 10.1021/jp300405x.

(17) Agarwal V, Dauenhauer PJ, Huber GW, Auerbach SM. Ab initio dynamics of cellulose pyrolysis: Nascent decomposition pathways at 327 and 600 °C. J Am Chem Soc. 2012;134(36):14958–72. doi: 10.1021/ja305135u.

(18) Hosoya T, Skaki S. Levoglucosan formation from crystalline cellulose: importance of a hydrogen bonding network in the reaction. ChemSusChem. 2013;6(12):2356–68. doi: 10.1002/cssc.201300338.

(19) Zhang Y, Liu C, Xie H. Mechanism studies on β-d-glucopyranose pyrolysis by density functional theory methods. J Anal Appl Pyrolysis. 2014;105(Jan):23–34. doi: 10.1016/j.jaap.2013.09.016.

(20) Murillo JD, Moffet M, Biernacki JJ, Northrup S. High-temperature molecular dynamics simulation of cellobiose and maltose. AIChE J. 2015;61(8):2562–70. doi: 10.1002/aic.14854.

(21) Zhang Y, Liu C, Chen X. Unveiling the initial pyrolytic mechanisms of cellulose by DFT study. J Anal Appl Pyrolysis. 2015;113:621–9. doi: 10.1016/j.jaap.2015.04.010.

(22) Zheng M, Wang Z, Li X, Qiao X, Song W, Guo L. Initial reaction mechanisms of cellulose pyrolysis revealed by ReaxFF molecular dynamics. Fuel. 2016;177(Aug.1):130–41. doi: 10.1016/j.fuel.2016.03.008.

(23) Zhang M, Geng Z, Yu Y. Density functional theory (DFT) study on the pyrolysis of cellulose: the pyran ring breaking mechanism.

Computational Theor Chem. 2015;1067:13–23. doi: 10.1016/j.comptc.2015.05.001.
(24) Li X, Tang C, Wang J, Tian W, Hu D. Analysis and mechanism of adsorption of naphthenic mineral oil, water, formic acid, carbon dioxide, and methane on meta-aramid insulation paper. J Mater Sci. 2019;54(11):8556–70. doi: 10.1007/s10853-019-03476-x.
(25) Miyamoto H, Yamane C, Ueda K. Molecular dynamics simulation of dehydration in cellulose/water crystals. Cellulose. 2015;22:2899–910. doi: 10.1007/s10570-015-0716-x.
(26) Ishikawa T, Hayakawa D, Miyamoto H, Ozawa M, Ozawa T, Ueda K. Ab initio studies on the structure of and atomic interactions in cellulose IIII crystals. Carbohydr Res. 2015;417:72–7. doi: 10.1016/j.carres.2015.09.006.
(27) Wang YY, Yang T, Liao RJ. Molecular dynamic simulations of glass transition temperature and mechanical properties in the amorphous region of oil-immersed transformer insulation paper. Int J Mod Phys B. 2012;26(19):9–479. doi: 10.1142/S0217979212501007.
(28) Li Y, Lin M, Davenport JW. Ab Initio Studies of Cellulose I: Crystal Structure, Intermolecular Forces, and Interactions with Water. JPhysChemC. 2011;115(23):11533–9. doi: 10.1021/jp2006759.
(29) Maurer RJ, Sax AF. Molecular dynamics of cellulose crystal surfaces with ChemShell. Procedia Computer Sci. 2010;1(1):1149–54. doi: 10.1016/j.procs.2010.04.128.
(30) Gilbert R, Jalbert J, Pierre TétreaultMorin, Denos B, Y. Kinetics of the production of chain-end groups and methanol from the depolymerization of cellulose during the ageing of paper/oil systems. Part 1: Standard wood kraft insulation. Cellulose. 2009;16(2):327–38. doi: 10.1007/s10570-008-9261-1.
(31) Laurichesse D, Bertrand Y, Tran-Duy C, Murin V. Ageing diagnosis of MV/LV distribution transformers via chemical indicators in oil. 2013 IEEE Electrical Insulation Conference (EIC). IEEE; 2013.
(32) Sergei L, John S, Giovanni C, Wander. Depolymerization processes in the thermal degradation of cellulosic paper insulation in electrical transformers. Polym Degrad & Stab. 1998;61(3):507–11. doi: 10.1016/S0141-3910(97)00249-8.
(33) Madhavan K, Murthy T, Sethuraman R. Estimation of degree of polymerisation and residual age of transformers based on furfural levels in insulating oil through generalized regression neural networks. Springer Berl Heidelb. 2006. doi: 10.1007/3-540-34783-6_7.
(34) Wang S, Guo X, Liang T, Zhou Y, Luo Z. Mechanism research on cellulose pyrolysis by Py-GC/MS and subsequent density functional theory studies. Bioresour Technol. 2012;104:722–8. doi: 10.1016/j.biortech.2011.10.078.
(35) Engel E, Dreizler RM. Density functional theory. Theoretical and Mathematical Physics; 2011.
(36) Hohenberg P, Kohn W. Density functional theory (DFT). Phys Rev. 1964. vol. 136, No. 1964, p. B864.
(37) Kohn W, Sham LJ. Self-consistent equations including exchange and correlation effects. Phys Rev. 1965;140(4A):A1133.
(38) Perdew JP, Chevary JA, Vosko SH, Jackson KA, Pederson MR, Singh DJ, et al. Atoms, molecules, solids, and surfaces: Applications of the generalized gradient approximation for exchange and correlation. Phys Rev B. 1992;46(11):6671. doi: 10.1103/PHYSREVB.46.6671.
(39) Bosko JT, Todd BD, Sadus RJ. Molecular simulation of dendrimers and their mixtures under shear: Comparison of isothermal-isobaric (NPT) and isothermal-isochoric (NVT) ensemble systems. J Chem Phys. 2005;123(3):541. doi: 10.1063/1.1946749.
(40) Ji J, Wang K, Zhu S, Zhu W. Structure, intermolecular interactions, and dynamic properties of NTO crystals with impurity defects: a computational study. CrystEngComm. 2021;23(12):2455–68. doi: 10.1039/D0CE01670E.